



HAL
open science

Overview of the U_3TGe_5 family with $T=Ti, V, Cr, Mn, Zr, Nb, Mo, Hf, Ta$ and W Nine new members, phase formation, stability, structural and physical properties and electronic structures

C. Moussa, N. Brisset, G. Chajewski, M. Samsel-Czekala, Pascal Boulet, H. Noël, M. Pasturel, A. Pikul, O. Tougait

► To cite this version:

C. Moussa, N. Brisset, G. Chajewski, M. Samsel-Czekala, Pascal Boulet, et al.. Overview of the U_3TGe_5 family with $T=Ti, V, Cr, Mn, Zr, Nb, Mo, Hf, Ta$ and W Nine new members, phase formation, stability, structural and physical properties and electronic structures. *Journal of Solid State Chemistry*, 2019, 277, pp.260-270. 10.1016/j.jssc.2019.06.017 . hal-02182248

HAL Id: hal-02182248

<https://univ-rennes.hal.science/hal-02182248>

Submitted on 12 Jul 2019

HAL is a multi-disciplinary open access archive for the deposit and dissemination of scientific research documents, whether they are published or not. The documents may come from teaching and research institutions in France or abroad, or from public or private research centers.

L'archive ouverte pluridisciplinaire **HAL**, est destinée au dépôt et à la diffusion de documents scientifiques de niveau recherche, publiés ou non, émanant des établissements d'enseignement et de recherche français ou étrangers, des laboratoires publics ou privés.

Overview of the U_3TGe_5 family with $T=Ti, V, Cr, Mn, Zr, Nb, Mo, Hf, Ta$ and W : nine new members, phase formation, stability, structural and physical properties and electronic structures.

Chantal Moussa^{1,4§}, Nicolas Brisset¹, Grzegorz Chajewski², Małgorzata Samsel-Czekala², Pascal Boulet³, Henri Noël¹, Mathieu Pasturel^{1,*}, Adam Pikul² and Olivier Tougait^{1,5§}.

¹Univ Rennes, CNRS, Institut des Sciences Chimiques de Rennes – UMR6226, 35042 Rennes Cedex, France

² Institute of Low Temperature and Structure Research, Polish Academy of Sciences, ul. Okólna 2, 50-422 Wrocław, Poland

³ Institut Jean Lamour, UMR CNRS 7198, Université de Lorraine, 54011 Nancy, France

⁴ School of Arts and Sciences, Department of Natural Sciences, Lebanese American University, Lebanon

⁵ Univ. Lille, CNRS, Centrale Lille, ENSCL, Univ. Artois, UMR 8181 - UCCS - Unité de Catalyse et Chimie du Solide, F-59000 Lille, France

§ present address

* Corresponding author : M. Pasturel, mathieu.pasturel@univ-rennes1.fr

Abstract :

Nine new ternary uranium transition metal germanides U_3TGe_5 with $T = V, Cr, Mn, Zr, Nb, Mo, Hf, Ta$ and W have been discovered, in addition to the previously reported compound for $T = Ti$. These ten intermetallics adopt the anti-CuHf₅Sn₃-type of structure (hexagonal, $P6_3/mcm$, $Z = 2$). Scanning electron microscopy images, energy dispersive spectroscopy, differential thermal analyses and X-ray refinements were employed for chemical, thermal and structural characterizations. For the purest samples, obtained for $T = Ti, V$ and Cr , the investigation of the magnetic and transport properties were analyzed revealing the subsequent influence of the $3d$ metals on the ground-state properties. *Ab initio* calculations of the band structure of these three U_3TGe_5 compounds were performed, showing nested Fermi surface which may be associated to the presence of Dirac cones for the magnetically ordered compounds, *i.e.* for $T = Ti$ and V .

Keywords: intermetallics, heavy fermion, magnetism, electrical resistivity, specific heat, electronic band structure.

1. Introduction

In recent years, the binary and ternary uranium germanides have been widely investigated due to their intriguing electronic properties. The most striking example is the coexistence of ferromagnetic and superconducting states encountered in UGe_2 ($T_C = 53$ K, $T_{SC} = 0.75$ K, under pressure, $P = 11.4$ kBar) [1], URhGe ($T_C = 9.5$ K, $T_{SC} = 0.25$ K) [2] and UCoGe ($T_C = 3$ K, $T_{SC} = 0.5$ K) [3]. In these compounds, the superconductivity and ferromagnetism are considered as cooperative phenomena and not as competing effects. Both transitions can be attributed to the $5f$ electrons only. It has been recognized that despite UGe_2 (ZrGa₂-type, orthorhombic, $Cmmm$) and UTGe , $T = \text{Co, Rh}$ (TiNiSi-type, orthorhombic, $Pnma$) adopt different crystal structures, they present similar features identified as (i) infinite U zig-zag chains with interatomic distances about 3.5 \AA at room temperature and (ii) ordered magnetic moments lying on the zig-zag chain planes [4].

Looking more closely to the ternary uranium germanides identified by our research group which may display similar structural and magnetic features to those above mentioned, the survey converged to U_3TiGe_5 [5]. This compound crystallizes in a hexagonal unit-cell (space group $P6_3/mcm$) with the anti-CuHf₅Sn₃ type. It presents infinite zig-zag chains of U atoms that are running along the c -axis, with interatomic distances of $3.462(1) \text{ \AA}$ at room temperature. It is a ferromagnet below $T_C = 76$ K with a canted magnetic structure showing ordered moments mainly aligned along the c -axis with reduced antiferromagnetically coupled contributions in the (a,b) hexagonal plane [5].

The anti-CuHf₅Sn₃-type adopted by U_3TiGe_5 is an inverse ternary ordered variant of the Ti_5Ga_4 -type [6] adopted by the uranium binaries U_5Sb_4 [7], U_5Sn_4 [8] and U_5Ge_4 [9]. This inverse arrangement is widely encountered in ternaries defined as $F\text{-}T\text{-}X$, with $F = 4f$ or $5f$ element, $T =$ early transition metal and $X = \text{Ge, Sn or Sb}$ [10] and more especially, it generates an extended family of isostructural uranium antimonides, U_3TSb_5 for $T = \text{Sc, Ti, Zr, Hf, V, Nb, Cr, and Mn}$ [11-13].

This structure type provides an interesting play-ground for the understanding of the relationships between structural and physical properties of U based intermetallics. Thus we decided to investigate the transport properties of U_3TiGe_5 and to explore its crystal chemistry by extending this family of ternary uranium germanides. For these prospecting syntheses, the transition-metals yielding the formation of the ternary uranium antimonide series were used as guidelines.

The present article reports about the formation of nine new ternary U_3TGe_5 uranium germanides with $T = Zr, Hf, V, Nb, Ta, Cr, Mo, W$ and Mn crystallizing with the anti- $CuHf_5Sn_3$ -type structure. For the purest samples obtained with the $3d$ metals, namely U_3TGe_5 with $T = V$ and Cr , some of their electronic properties are given, along with the transport properties of U_3TiGe_5 which have never been reported up to now. Furthermore, a comparative study between the band structure, electronic structure, total and partial densities of states for the three U_3TGe_5 with $T = Ti, V$ and Cr is presented. Altogether, the experimental and computational results sketch a complete picture about the physical properties of this family of compounds.

2. Experimental and computational details

Starting materials were turnings of U (99.7 %, CETAMA, batch 'Jonquille'), Ti (Alfa Aesar, 99.9%), V (Alfa Aesar, 99.9 %), Cr (Strem, 99.99 %), Mn (Strem, 97 %) Zr (Strem, 99.8 %), Nb (Strem, 99.8 %), Mo (Alfa Aesar, 99.999 %), Hf (Strem, 99.5 %), Ta (Strem, 99 %) and powders of W (Alfa Aesar, 99.95 %), Re (Alfa Aesar, 99.99 %), and Ge pieces (Strem, 99.999 %). The elements were mixed in stoichiometric ratio and were melted in an arc-furnace under a Ti/Zr gettered argon atmosphere. The cold buttons were turned and re-melted three times at least to ensure a proper melting of the phase constituents. The resulting ingots were characterized in as-melted state or heat-treated states after two distinct annealing procedures. Long-term annealing was performed at temperatures below 1200 K for dwell periods ranging from two to four weeks. For that, the ingots were introduced in silica tubes which were evacuated under residual argon atmosphere before being flame sealed and placed in resistance furnace. Short-term annealing was carried out in the temperature range 1473-1673 K for about 6 hours. For this second type of heat treatment, the master ingots were placed under low Ar -pressure into a water-cooled copper crucible surrounded by the working coil connected to a high-frequency generator. The electrical power was increased until the target temperature, measured by an IR-bichromatic pyrometer, was reached.

Each bulk sample was analyzed by powder X-ray diffraction collected at room temperature using a Bruker AXS D8 Advance diffractometer (θ - 2θ Bragg-Brentano geometry, monochromatized $Cu K\alpha_1$ radiation, $\lambda = 1.5406 \text{ \AA}$), equipped with a LynxEye fast detector. The experimental diffraction patterns were analyzed with the help of the Le Bail and Rietveld methods implemented in the FullProf suite [14].

The microstructure of the samples was examined on polished surfaces using a Jeol JSM 7100F scanning electron microscope (SEM) equipped with a silicon drift detector energy dispersive spectrometer (EDS) - X-Max 50 from Oxford Instrument - employed for the elemental analysis of the various phases. Elemental compositions were obtained by averaging the values of at least three EDS analyzed zones, from different areas of the sample. An estimated deviation from the mean value is about 1 at.%.

Differential thermal analysis (DTA) was performed on a Setaram LabSys 1600 apparatus, calibrated using the phase transitions and melting temperatures of different pure metals (Al, Cu and Fe). The measurements were performed in alumina crucibles up/down, to/from 1873 K at heating/cooling rates of 5, 10 or 20 K min⁻¹, under a 5 N purity argon flow.

Small single crystals suitable for crystal structure determination were picked up from the heat-treated samples. The diffraction intensities were collected at room temperature on a Nonius Kappa CCD four circle diffractometer working with Mo K α radiation ($\lambda = 0.71073$ Å). The integration and reduction of redundant reflections of the different data sets as well as the cell refinements were performed using the SADABS software [15]. All the structure refinements and Fourier syntheses were made with the help of SHELXL-13 [16].

The magnetic properties were studied in temperature range 2-300 K and magnetic fields up to 5 T using a Quantum Design SQUID magnetometer. The specific heat and electrical resistivity were measured at temperatures from 2 to 300 K using a Quantum Design PPMS platform.

The electronic structures of U₃TGe₅ systems with $T = \text{Ti, V, Cr}$ have been calculated employing the fully relativistic version of the full-potential local-orbital (FPLO) method [17], which includes all relativistic effects such as the spin-orbit (SO) coupling. The local density or spin density approximation (LDA) or (LSDA) [18] of the exchange-correlation functional was applied without or with spin-polarization. In addition orbital polarization correction (LSDA+OPC) [19] were implemented to the U 5*f* states, along with generalized gradient approximation (GGA) [20]. The electronic configurations of atoms used in the calculations were the valence electrons automatically selected by the internal procedure. The experimental lattice parameters and atomic positions of U₃CrGe₅ and U₃VGe₅ (gathered in Tables 2 and 3) were used whereas the structural data of U₃TiGe₅ were taken from [5]. The FPLO code yielded the Mulliken decomposition of charges, which is somewhat dependent on the orbital used. The $12 \times 12 \times 12$ size of the selected \mathbf{k} -point meshes corresponded to 133 points in the irreducible wedge of the Brillouin zone (BZ). The band structures, total and partial densities

of states (DOSs), and Fermi surfaces (FSs) were computed. The partial DOSs were obtained for different atomic sites or electron orbitals and plotted per formula unit (f.u.).

3. Results

3.1 Phase formation

All the ingots were prepared by arc-melting the elemental components with the nominal composition U_3TGe_5 for $T = Sc, Ti, V, Cr, Mn, Y, Zr, Nb, Mo, Hf, Ta, W$ and Re . The phase formation and the purity of the samples were examined by means of powder XRD and SEM-EDS analyses for the as-cast and heat-treated states.

The $CuHf_5Sn_3$ antitype structure can be readily obtained by direct solidification of the melt with a yield above 95 % for $T = Ti, V, Cr$ and Mo . The impurity phases were identified as the binary uranium germanides, UGe_2 or UGe_3 for $T = Ti$ and V and as some traces of the ternary compounds $U_2T_3Ge_4$ [21] for $T = Cr$ and Mo . For the samples with $T = Mn, Zr, Nb, Hf, Ta$ and W , the anti- $CuHf_5Sn_3$ type was observed in medium to low yield, but systematically in presence of two secondary phases, at least. These secondary phases are mainly the ternary extensions of the binary uranium germanides UGe [22] and UGe_2 [23] and the ternary phases $U_2T_3Ge_4$ for $T = Nb, Ta, Zr$ and W [24, 25] and UMn_2Ge_2 [26]. The samples with $T = Sc$ and Y exhibit blurred microstructures comprising large zones of a fine-grain eutectic phase. The corresponding powder X-ray diffractograms show complicated patterns. Only the main diffraction peaks could be indexed according to an AlB_2 type of unit-cell. For the sample with starting composition $3U-1Re-5Ge$, after subtracting the diffraction peaks of binary uranium germanides, our efforts to index the remaining peaks were fruitless. The SEM-EDS analyses confirm the polyphasic nature of the sample, with binary uranium germanides and a ternary phase having an elemental composition of about $25U-34Re-41Ge$ in at. %.

Examination of the samples annealed at intermediate temperatures (below 1200 K) for dwell periods up to four weeks mainly revealed grain growth, but with rather similar features in term of phases in presence compared to the as-cast state, except for $T = Mn$. For this metal a relevant increase of the U_3MnGe_5 content is observed, but still with the presence of the ternary extensions of UGe_2 and UGe and UMn_2Ge_2 ternary compound. Regarding the samples with $T = Sc$ and Y , the microstructural refinement associated to the heat-treatment yields samples with improved crystalline features and large homogeneous zones needed for precise investigations. Obviously, they indicate the unsuccessful synthesis of the inverse $CuHf_5Sn_3$ phases with these two metals. For the samples with the other transition metals, $T = Ti, Cr, V,$

Zr, Nb, Mo, Hf, Ta and W, these long-term annealing processes were useless to remove the traces of the impurity phases for $T = \text{Ti, V, Cr}$ and Mo and to promote further solid state formation of the U_3TGe_5 phase for $T = \text{Zr, Nb, Hf, Ta}$ and W.

The high temperature heat-treatments were also found inefficient to get rid of the impurity phases in the samples with $T = \text{Ti, V, Cr}$ and Mo, but rather efficient to activate the formation of the U_3TGe_5 phase with the refractory metals $T = \text{Zr, Nb, Hf, Ta}$ and W. In these samples, the U_3TGe_5 phase was found to be the major product, but still with detectable secondary phases. The sample with nominal composition '3U-1Re-5Ge' presents similar phases as observed for the as-cast state, confirming the unsuccessful formation of the U_3TGe_5 phase with this transition metal.

To summarize, the presence of U_3TGe_5 with $T = \text{Ti, V, Cr, Mn, Zr, Nb, Mo, Hf, Ta}$ and W was observed in as-cast ingots suggesting that the formation mode occurs through a reaction which may involve a liquid phase. The long-term heat-treatments performed at intermediate temperature mostly induce microstructural refinements without significant effect on the U_3TGe_5 content in the samples, excluding a peritectoid mode of formation. Finally the short-term heat-treatments at rather high temperature thermally activate the diffusion to promote the formation of U_3TGe_5 phases, especially for the refractory metals. All these observations suggest a peritectic mode of formation of U_3TGe_5 . To ascertain this point, DTA measurements were performed at temperatures up to 1823 K.

3.2 Thermodynamic behavior

DTA curves were recorded on heating and cooling for the purest samples of U_3TGe_5 with $T = \text{Ti, Cr, V, Mn, Zr, Nb, Mo, Hf}$ and Ta. It should be noticed that the liquidus and solidus temperatures could be hardly recognizable. For most of the samples, with $T = \text{Ti, V, Cr, Mn, Zr, Nb}$ and Mo, the curves show several endothermic and exothermic peaks with noticeable temperature shifts between heating and cooling modes, suggesting cascades of peritectic transformations. Most of the endothermic peaks occur in a narrow temperature domain ranging from 1660-1740 K. This temperature zone corresponds to the range of the extensive transformations existing in the U-Ge binary system for 50-75 at.% Ge [27] which therefore hampers a straightforward assignment for most of the transitions.

For the *5d* transition metals ($T = \text{Hf, Ta}$ and W) any significant endothermic peak can be detected, indicating that the U_3TGe_5 phase with these refractory metals has a decomposition temperature above 1823 K. It also confirms that the series of endothermic peaks observed for

the other metals results from successive peritectic reactions. Based on microstructural analyses, it can be postulated that U_3TGe_5 phases decompose by peritectic reaction yielding a binary U-Ge compound, most presumably being UGe_2 and a ternary $U_xT_yGe_z$ phase, most presumably being $U_2T_3Ge_4$ for $T = Ti, V, Cr, Zr, Nb$ and Mo , at least.

The temperature of the peritectic decomposition was defined as the onset of the first endothermic peak. The transition temperatures are summarized in Table 1.

3.3 Crystal structure

The U_3TGe_5 family with $T = Ti, V, Cr, Mn, Zr, Nb, Mo, Hf, Ta$ and W crystallizes in the $P6_3/mcm$ space group (no. 193) and adopts the anti- $CuHf_5Sn_3$ type of structure. The crystal structure of U_3VGe_5 and U_3CrGe_5 was refined from single crystal XRD data, with single crystals extracted from crushed annealed ingots. The atomic positions of U_3TiGe_5 [5] were taken as initial structural model. Some refined crystal parameters and further details of the data collections are summarized in Table 2. Final values of the positional and displacement parameters are given in Table 3. As an illustration of this crystal structure often described in the literature [11-13 and references therein], the unit-cell of U_3VGe_5 is shown in Fig. 1a. The transition metal atoms are 6 coordinated by Ge atoms in a regular octahedral geometry whereas the U atoms are surrounded by 9 Ge atoms which form a heavily distorted tricapped trigonal prism. Two adjacent $[UGe_9]$ polyhedra condense by sharing a triangular face. Along the c -direction, the anti- $CuHf_5Sn_3$ type is characterized by infinite linear chains of T atoms resulting from the face-sharing of $[TGe_6]$ octahedra and infinite U zig-zag chains within Ge tunnels of rhombus section. The interatomic distances within the linear chains of T atoms correspond to half c parameter. The zig-zag U-chains (Fig.1b) display an almost constant angle of $111(1)^\circ$ for interspacing ranging from $3.426(1)$ for $T = Cr$ to $3.523(1)$ for $T = Zr$. Comparing with the U-chains in ferromagnetic superconductors, these distances are significantly smaller than those in UGe_2 ($d_{U-U} \approx 3.82 \text{ \AA}$) but in the range of those found in $UCoGe$ and $URhGe$ ($d_{U-U} \approx 3.48$ and 3.50 \AA , respectively), while the angle is intermediate between those in the binary ($\approx 63.8^\circ$) and the ternaries ($\approx 156 - 160^\circ$). In the (a,b) plane (Fig. 1c) the U atoms form a triangular network with two distinct U-U distances, short ones being below 4.6 \AA (solid line) and the long ones being about 5.6 \AA (dotted line).

The lattice parameters of the nine new phases along with the ones of U_3TiGe_5 were refined from powder XRD data using a global approach for the fitting of profile parameters on multiphase samples. Table 4 gathers the lattice parameters of the family of germanides, and

Fig. 2 displays their evolution as the function of the metallic radius of the transition metal (r_T) outlining a monotonic trend with the exception of $T = \text{Mn}$. For the uranium antimonides U_3TSb_5 [11-13], similar features are observed in terms of a smooth expansion of the lattice parameters with r_T and an anomaly for $T = \text{Mn}$. For both series of compounds, the lattice parameters and the unit-cell volume for all the compounds remain in narrow ranges, pointing out steric effects as important factors in the phase formation of the ternary compounds with the anti- CuHf_5Sn_3 -type of structure.

3.4 Physical properties

For the purest samples, *i.e.* those containing more than 95 vol. % of the U_3TGe_5 phase, obtained for the $3d$ metals ($T = \text{Ti}, \text{V}, \text{Cr}$) a detailed study of the electronic properties was carried out. The transport and magnetic properties were investigated by means of electrical resistivity, specific heat, *dc* and *ac*-susceptibilities. Their results are presented in the following subsections and fitting parameters summarized in Table 5.

3.4.1 Magnetic properties

Fig. 3a displays the inverse molar magnetic susceptibility of U_3VGe_5 as a function of temperature. Above about 40 K, the $\chi_{\text{mol}}^{-1}(T)$ curve exhibits a nearly linear behavior and can be described by a modified Curie-Weiss law:

$$\chi_{\text{mol}}(T) = \chi_0 + \frac{C}{T - \theta_p} \quad (1)$$

where C is the Curie constant, θ_p is the paramagnetic Curie-Weiss temperature and χ_0 is the temperature independent contribution of Pauli paramagnetism of conduction-band electrons and core diamagnetism. Least-squares fits of equation (1) to the experimental data yield the values $C = 20.9 \text{ cm}^3 \text{ K mol}^{-1}$, $\theta_p = 23 \text{ K}$ and $\chi_0 = 3.08 \cdot 10^{-2} \text{ cm}^3 \text{ mol}^{-1}$. The effective magnetic moment $\mu_{\text{eff}} = \sqrt{\frac{3Ck_B}{n\mu_0 N_A}}$ (where μ_0 , N_A and k_B are the magnetic permeability of free space, the Avogadro's number and the Boltzmann's constant, respectively, and n is a number of magnetic moments per formula unit) is equal to $2.64 \mu_B$ per U-atom. Such value is much lower value than those expected for $5f^3$ configuration of U^{3+} and $5f^2$ configuration of U^{4+} free ions ($3.62 \mu_B$ and $3.58 \mu_B$ respectively), and hence it suggests the partial delocalization of the magnetic moments of uranium, being in line with the observed positive and non-negligible value of χ_0 . However, it should be taken into account that this approach neglects completely

the crystal field effect, which is usually present in uranium intermetallics and can also lead to the reduction of the effective magnetic moment.

Despite the positive value of θ_p , suggesting predominant ferromagnetic interactions between the magnetic moments of uranium atoms, U_3VGe_5 orders antiferromagnetically at the Néel temperature $T_N = 25$ K, which is manifested as a distinct cusp-like anomaly in temperature variation of the molar magnetization $M_{mol}(T)$ (upper inset to Fig. 3a). Some bifurcation of the $M_{mol}(T)$ curves between the zero-field-cooling (ZFC) and field-cooling (FC) regimes suggests the presence of a tiny ferromagnetic contribution. Such a contribution may result from a small tilt between antiparallel ferromagnetic layers, associated with a canted magnetic structure.

Field dependence of the magnetization confirms the antiferromagnetic character of the ordering (lower inset to Fig. 3a). In particular, below about 1 T the magnetization of U_3VGe_5 increases linearly with rising $\mu_0 H$, as expected for antiferromagnets. Subsequent rapid increase of M_{mol} with some magnetic hysteresis between about 1 and 3 T, followed by clear tendency to saturation in higher fields, manifests field-induced metamagnetic phase transition from an antiferromagnetic to a ferromagnetic-like state. Assuming that at 5 T a single-domain model with all the magnetic moments parallel oriented is achieved, the measured value of $M_{mol}(5T) = 12.4$ J T⁻¹ mol⁻¹ yield the magnitude of the ordered magnetic moment μ_{ord} as being equal to $2.22 \mu_B$ per formula unit (i.e. $0.74 \mu_B$ per U-atom). This significantly reduced value may be correlated to crystal field effect in the compound, as already hypothesized.

Results of the magnetization measurements carried out in various magnetic fields (Fig. 3b) confirm the magnetic properties of U_3VGe_5 : the curves measured at 0.1 and 0.5 T have clearly antiferromagnetic character, while $M(T)$ measured at 4 T shows smeared Brillouin-like shape characteristic of field-induced ferromagnets. Temperature variation of the *ac*-magnetic susceptibility of U_3VGe_5 measured in zero magnetic field (inset to Fig. 3b) exhibits distinct anomaly in the real part of the susceptibility (χ') associated with featureless imaginary component (χ''), hence confirming the antiferromagnetic ground state of the compound.

Magnetic properties of U_3CrGe_5 are summarized in Fig. 4. At high temperatures the inverse molar susceptibility of the compound can be described by the modified Curie–Weiss law (Eq. 1) with the fitting parameters $C = 23.2$ cm³ K mol⁻¹ (yielding $\mu_{eff} = 2.22 \mu_B$), $\theta_p = -54$ K and $\chi_0 = 3.54 \times 10^{-2}$ cm³ mol⁻¹. The effective magnetic moment is even lower than in U_3VGe_5 , which is also in line with larger χ_0 . Enlarged negative paramagnetic Curie-Weiss temperature points to an antiferromagnetic character of the interactions between the magnetic

moments. Downward deviation of the experimental curve from the Curie-Weiss law is clearly seen below about 120 K followed by an upturn in the $\chi_{\text{mol}}(T)$ curve at the lowest temperatures (upper inset to Fig. 4). The upturn could be ascribed to ferromagnetic-like ordering at about 25 K, being in line with some ferromagnetic hysteresis observed in $M(H)$ (lower inset to Fig. 4). However, no trace of any phase transition was detected in either specific heat or electrical resistivity data (see below). This leads us to the conclusion that the observed low-temperature magnetic properties are most probably not intrinsic.

3.4.2 Specific heat

Fig. 5 shows the specific heat C_P of U_3TiGe_5 , U_3VGe_5 and U_3CrGe_5 measured as a function of temperature in zero magnetic field. Experimental curves collected for the two former phases show distinct anomalies corroborating the bulk ferromagnetic ordering in U_3TiGe_5 at $T_C = 73$ K and the antiferromagnetic one in U_3VGe_5 at $T_N = 25$ K, being in perfect agreement with the other measured physical properties. As mentioned above, no anomaly has been found in $C_P(T)$ of U_3CrGe_5 , which confirms the absence of long-range magnetic ordering of the compound. Due to a lack of an isostructural nonmagnetic reference, a further analysis of the specific heat of all the studied systems must be limited to very low temperatures, at which the phonon contribution to the specific heat follows the conventional Debye T^3 -law:

$$\frac{C_P}{T} = \gamma + \beta T^2 \quad (2)$$

where γ is the Sommerfeld coefficient and $\beta = 1944 \frac{r}{\Theta_D^3}$ (r – number of atoms in the formula unit, Θ_D – Debye temperature) [28].

As can be inferred from the lower inset to Fig. 5, the $C_P(T)$ curves of U_3TiGe_5 and U_3VGe_5 (plotted as C_P/T vs. T^2) show linear behavior below about 6 K. This low temperature domain can be described by Eq. 3 where the second term of Eq. 2 is developed for the magnon contribution in magnetically ordered system. Only for U_3TiGe_5 where the ordering temperature is relatively high, it can be assumed that contribution of the ferromagnetic magnons is negligible in the considered fitting range (ratio about 12). Least-square fits of Eq. 2 to the experimental data (see the lower inset to Fig. 5) yielded the parameters $\gamma = 105 \text{ mJ mol}^{-1} \text{ K}^{-2}$ (or $35 \text{ mJ mol}_U^{-1} \text{ K}^{-2}$) and $\beta = 0.7 \text{ mJ mol}^{-1} \text{ K}^{-4}$ for U_3TiGe_5 . The Debye temperature, estimated using the latter parameter, is equal to 292 K, which is quite reasonable value for uranium germanides [29]. The moderately enlarged γ value suggests the presence of some electronic correlations in U_3TiGe_5 .

In U_3VGe_5 the ordering temperature is much lower. Therefore the contribution of the antiferromagnetic magnons cannot be neglected in the fitting range. In fact, the slope of the linear dependence in C_p/T vs. T^2 of this compound is larger than in the system with Ti. Assuming that Θ_D of all three isostructural systems is nearly the same, one can fit the $C_p(T)/T$ curve of U_3VGe_5 by the formula:

$$\frac{C_p}{T} = \gamma + \beta T^2 + \alpha_{AFM} T^2 \quad (3)$$

in which the third term describes conventional antiferromagnetic magnons contribution to the specific heat [28] and β is fixed on the value obtained for U_3TiGe_5 . The least-squares fits of Eq. 3 to the experimental data yielded for U_3VGe_5 the parameters $\gamma = 340 \text{ mJ mol}^{-1} \text{ K}^{-2}$ (or $113 \text{ mJ mol}_U^{-1} \text{ K}^{-2}$) and $\alpha_{AFM} = 0.9 \text{ mJ mol}^{-1} \text{ K}^{-4}$ (lower inset to Fig. 5). It is worth noting that the γ coefficient of the V-bearing system is more than three times larger than in U_3TiGe_5 , which suggests stronger electron-electron interactions in the former compound, being in line with its lower magnetic ordering temperature.

As can be seen in the upper inset to Fig. 5, the low-temperature behavior of the specific heat of U_3CrGe_5 differs from that observed in U_3TiGe_5 and U_3VGe_5 : it shows a distinct increase in $C_p(T)/T$ with decreasing T . Such an upturn can be considered as manifesting critical spin fluctuations associated with magnetic phase transition at absolute zero temperature. Indeed, the experimental data seem to follow the theoretical predictions for such systems – they can be described by the formula:

$$\frac{C_p}{T} = \gamma^* + \beta^* T^2 + \delta T^2 \ln T \quad (4)$$

where $\beta^* = \beta - \delta \ln T_{sf}$ and γ^* is the γ coefficient enhanced by rising an effective mass of conduction electron due to the fluctuation process (cf. *e.g.* [30, 31]). Least-squares fit of Eq. 4 to the experimental data (solid line in the upper inset to Fig. 5) yielded the parameters $\gamma^* = 510 \text{ mJ mol}^{-1} \text{ K}^{-2}$ (or $170 \text{ mJ mol}_U^{-1} \text{ K}^{-2}$), $\beta^* = -6.6 \text{ mJ mol}^{-1} \text{ K}^{-4}$ and $\delta = 2.8 \text{ mJ mol}^{-1} \text{ K}^{-4}$. Using β parameter found for U_3TiGe_5 one can estimate the spin fluctuations temperature T_{sf} as to about 14 K. The value of γ^* in U_3CrGe_5 is similar to the reported ones for UGe ($137 \text{ mJ mol}_U^{-1} \text{ K}^{-2}$) [29] and the canonical spin fluctuator $UA1_2$ ($145 \text{ mJ mol}_U^{-1} \text{ K}^{-2}$) [32].

3.4.3 Electrical resistivity

Fig. 6a displays temperature dependences of the electrical resistivity $\rho(T)$ of U_3TiGe_5 ,

U_3VGe_5 and U_3CrGe_5 . Above about 100 K $\rho(T)$ of all three compounds are weakly temperature dependent. At low temperatures distinct anomalies followed by a drop of ρ confirm the bulk magnetic ordering of U_3TiGe_5 and U_3VGe_5 at $T_C = 73$ K and $T_N = 25$ K, respectively. The anomalies are well visible also in the first derivative of the resistivity $d\rho/dT$ of both compounds displayed in the inset to Fig. 6a. The lack of any sharp anomaly in $\rho(T)$ as well as in $d\rho(T)/dT$ of U_3CrGe_5 is in agreement with its featureless specific heat and thus supports a paramagnetic ground state for this compound. In turn, the overall shape of the $\rho(T)$ curve of U_3CrGe_5 is characteristic of intermetallic systems exhibiting spin fluctuations, as *e.g.* UAl_2 [33], UPt_3 [34], UNi_2Al_3 [35] and many actinide or lanthanide Laves phases [36]. Hence it strongly bears out our hypothesis on the presence of spin-fluctuations in U_3CrGe_5 .

As can be inferred from Fig. 6b, $\rho(T)$ of the ferromagnetically ordered U_3TiGe_5 follows in the ordered region the theoretical predictions for electron scattering on ferromagnetic magnons. In particular, the $\rho(T)$ curve can be described below about 35 K by the formula developed for anisotropic ferromagnets [37]:

$$\rho(T) = \rho_0 + aT^2 + bT\Delta\left(1 + \frac{2T}{\Delta}\exp\left(-\frac{\Delta}{T}\right)\right) \quad (5)$$

where ρ_0 is the residual resistivity, the second term describes the electron-electron scattering, and the last term represents the scattering of the conduction electrons on magnons with a Δ gap in the magnon spectrum. Least-squares fit of Eq. 5 to the experimental data (solid line in Fig. 6b) yielded the parameters $\rho_0 = 40.8 \mu\Omega \text{ cm}$, $a = 0.074 \mu\Omega \text{ cm K}^{-2}$, $b = 0.346 \mu\Omega \text{ cm K}^{-2}$ and $\Delta = 92$ K.

Performing analogical analysis for the antiferromagnetically ordered U_3VGe_5 would not be reliable due to the too low value of T_N . As a consequence, the drop of the resistivity is not fully developed in the studied temperature range.

3.5 Electronic band structure.

The fully relativistic total and partial DOS's of non-magnetic (LDA) states of U_3TGe_5 systems with $T = \text{Ti}$, V and Cr , are displayed in Fig. 7. The overall metallic-like DOS's are similar for the three compounds, showing that valence electrons of all the constituent atoms, U $5f$ ($6d$), Cr/Ti/V $3d$, Ge $4sp$, are present at the Fermi level (E_F). However, in this region, located between the Fermi level and about -3 eV of the binding energy, the predominant peaks come from the U $5f_{5/2}$ states, originating from the three U atoms per f.u. They are distant by about 1.0 eV from the unoccupied U $5f_{7/2}$ ones and are slightly delocalized due to

hybridization with the T $3d$ states. The calculated Sommerfeld coefficients are relatively large with comparable values of $\gamma_b = 72.2, 74.5, 84.0$ mJ mol⁻¹ K⁻² per f.u. for $T = \text{Ti}, \text{V}$ and Cr , respectively. The continuous increase in the relative ratio of the corresponding experimental specific-heat values to the calculated ones, $\gamma/\gamma_b = 1.5, 4.6, 6.1$, reflects well established electronic features for U-based intermetallics. The lowest fraction factor of 1.5 obtained for U_3TiGe_5 , is typical of weakly correlated electron systems [38] whereas the highest one but still moderate factor of 6.1 obtained for U_3CrGe_5 outline the presence of spin fluctuations.

For the three electronic structures, it has been found that the uranium atoms transfer some electrons (~ 1.65 per U at.) to Ge ones lowering among others the numbers of $5f$ electrons N_{5f} from the nominal value 3 to about 2.75. Similarly, the nominal numbers of the valence electrons of the T atoms, $N_{\text{val}} = N_{3d} + N_{4s} = 4, 5$ and 6 for $T = \text{Ti}, \text{V}$ and Cr , respectively were found systematically smaller than expected, with values of $N_{\text{val}} = 3.11, 4.17$ and 5.41 . The origin of the significant reduction of the DOS of the T atoms at the vicinity of the Fermi level resides in two additive effects, (i) the hybridization of the T $3d$ wave-functions with the U $5f(6d)$ and Ge $4sp$ ones and (ii) some charge transfer from the T atoms to the Ge ones. The part of the charge transfer remains almost constant among the three transition metals, whereas the hybridization effect increases from Ti to V and to Cr, (with increasing the real number of $3d$ electrons) as illustrated in Fig. 7. Such evolution of the hybridization effect arising from the T atoms may reflect the change of the magnetic behaviour of the three compounds.

Assuming collinear magnetic moments along the c axis, some ferromagnetic states (FM) have successfully been obtained self-consistently, using different exchange-correlation functionals, only for U_3TiGe_5 and U_3VGe_5 . However, for LSDA and GGA applied to both systems, the total ordered uranium magnetic moments (all given per U-atom and oriented along the c axis), are almost zero (0.01 and $0.2 \mu_B$, respectively), resulting from an almost complete cancellation of their spin and orbital moments due to an anti-parallel coupling. Only LSDA+OPC functional yields reasonable values of a total U magnetic moment. For U_3TiGe_5 , it is equal to $1.15 \mu_B$ (with spin $1.70 \mu_B$ and orbital $-2.85 \mu_B$ contributions), in agreement with the reported experimental neutron-diffraction value of $1.00(7) \mu_B$ [5]. Similarly, for U_3VGe_5 the total ordered uranium magnetic moment amounts to $1.09 \mu_B$ (with spin $1.75 \mu_B$ and orbital $-2.84 \mu_B$ moments) in line with the field-induced FM state, detected in the magnetization measurements (Fig. 3a). The occurrence of magnetic moments carried by U-atoms only is in agreement with the results obtained for the isostructural compound U_3ZrSb_5 , studied by different band structure methods [39].

Fig. 8 presents the spin-polarized DOS's of both U_3TiGe_5 and U_3VGe_5 compounds in the FM states calculated with LSDA+OPC. In the vicinity of E_F , the U spin-up channels are much higher than the spin-down ones, yielding almost half-metallic systems. The corresponding bandplots, displayed in Figs. 9b and c in the expanded scales for LSDA+OPC, exhibit many peculiarities of Dirac-cone-like structures around E_F , as enlightened by red circles. Their non-trivial topologies which bear some resemblance with the band structure of the twisted graphene lattices [40] is very unique for uranium systems. Noteworthy, these features of the band structure in the ordered state are lacking in the paramagnetic one *i.e.* in the nonmagnetic (LDA) states for all three compounds as depicted in the bandplots calculated for U_3CrGe_5 in Fig. 9a. However, the assumption of the presence of the Dirac-cones needs further experimental evidence by means of angle-resolved photoelectron spectroscopy (ARPES) measurements, as an example.

Fig. 10(a-c) display the computed (LDA) Fermi surfaces of the three compounds U_3TGe_5 comprising as many as five or even six (for $T = V$) sheets which originate from Kramers double-degenerate bands. The sheets coming from the lower bands form hole-like closed pockets, centred at the Γ point, which possess different volumes and possible necks along the ΓM line. Conversely, the sheets derived from the upper bands have electron-like character and are open within hexagonal planes in the BZ. The situation is radically changed for the FS sheets obtained with LSDA+OPC for the magnetically ordered phases with $T = Ti$ and V as seen in Fig. 10(d,e). Although now the number of FS sheets, originating from bands with lifted up Kramers degeneracy, increased only by one for each compound but the majority of the sheets changed their topology from three-dimensional to quasi-one-dimensional. Namely, they are almost planar within the hexagonal planes as if metallic interactions were reduced mainly to directions parallel to the c axis, probably due to some orbital ordering along the U zig-zag chains.

4. Discussion / Conclusion

The series of ternary uranium transition metal germanides, U_3TGe_5 crystallizing with the inverse $CuHf_5Sn_3$ -type (hexagonal, $P6_3/mcm$ space group) have been extended by nine new members with $T = V, Cr, Mn, Zr, Nb, Mo, Hf, Ta$ and W , in addition to the previously reported one, U_3TiGe_5 . All the compounds readily form with transition metal, T of column 4 to 7, with this exception of Re. Our efforts to prepare an analogous ternary uranium

germanide with $T = \text{Sc}$ (column 3) were unsuccessful despite an isotypical compound existing in the ternary uranium antimonide series. The lattice parameters of the uranium germanide family linearly evolve with the metallic radius of the transition metals, as similarly observed for the U_3TSb_5 compounds. It emphasizes that the germanide and antimonide branches of these U-based isostructural compounds form for early transition metals according to both steric effects related to the T/X ($X = \text{Ge}, \text{Sb}$) atomic radius ratios and electronic count of the transition metals in the sense of electron poor metals.

Combined investigations of metallographic observations using SEM images, semiquantitative analyses by EDS, identification of phase transitions by DTA and single-crystal refinements indicate that the ternary uranium transition metal germanides, U_3TGe_5 should be regarded as line-compounds forming by peritectic reaction. The phase formation involves at least a binary uranium germanide, being most probably UGe_2 , as solid phase. The transformation may occur with the $\text{U}_2\text{T}_3\text{Ge}_4$ compounds as second solid phase, for $T = \text{Cr}, \text{Zr}, \text{Nb}, \text{Mo}, \text{Hf}, \text{Ta}$ and W at least. The reaction temperatures were evaluated above 1529(5) K which constitutes the lowest decomposition temperature found for $T = \text{Mn}$.

The electronic properties were measured by means of *ac* and *dc* susceptibilities, electrical resistivity and specific heat on polycrystalline samples for $T = \text{Ti}, \text{V}$ and Cr having a U_3TGe_5 phase content above 95 vol.%. In the absence of a non-magnetic analogue to extract the lattice contribution, a single value of the Debye temperature, $\Theta_{\text{D}} = 292 \text{ K}$, was assigned for all these isostructural ternary uranium germanides. This value was extracted from the specific heat of U_3TiGe_5 , by considering a modified Debye model which includes the magnon contribution, at very low temperature. Our measurements confirm the ferromagnetic ordering of U_3TiGe_5 below $T_{\text{c}} = 73(1) \text{ K}$, and establish for the first time its thermal and electrical resistivity behaviors. The Sommerfeld coefficient $\gamma = 35 \text{ mJ mol}_{\text{U}}^{-1} \text{ K}^{-2}$ evaluated from specific heat suggests moderate electron correlations at low temperature.

U_3VGe_5 has to be regarded as an antiferromagnet below $T_{\text{N}} = 25 \text{ K}$, but with an imperfect antiferromagnetic arrangement of the magnetic moments at low temperature. A spin-flip transition associated to a narrow hysteresis loop is observed between 1 and 3 T in the isothermal magnetization curves measured at $T = 2 \text{ K}$. The magnetic ordered moment per U-atom amounts to $0.74 \mu_{\text{B}}$. In the paramagnetic domain, the effective magnetic moment per U-atom amounts to $2.64 \mu_{\text{B}}$, a rather reduced value also. From the specific heat measurement a moderately large Sommerfeld coefficient, $\gamma = 113 \text{ mJ mol}_{\text{U}}^{-1} \text{ K}^{-2}$ was estimated, indicating stronger electronic correlations than in U_3TiGe_5 .

The paramagnetic ground state of U_3CrGe_5 is clearly brought out in all the physical measurements. The temperature dependence of the electrical resistivity displays a concave down curve, which is reminiscent of metallic systems with strong spin fluctuations. The low temperature evolution of the specific heat follows a typical model developed for spin fluctuations near magnetic ordering. The estimated Sommerfeld coefficient $\gamma = 145 \text{ mJ mol}_U^{-1} \text{ K}^{-2}$ obtained from the low temperature behaviour of specific heat qualifies U_3CrGe_5 as a moderate heavy fermion.

The considerable enhancement of the effective mass of conduction electrons at low temperatures along with a constant decrease of the magnetic exchange interactions when increasing the number of valence electrons of the $3d$ -transition metals *i.e.* from Ti to Cr, suggested an increase of the uranium f -electron hybridization with the p - and d -electrons from germanium and the $3d$ -transition metals.

Within this $3d$ -element series, the U-U distances (from about 3.42 \AA for $T = Cr$ to 3.48 \AA for $T = Ti$) and angles (about 111°) along the U-zig-zag chains are almost the same and cannot thus be considered as the main driving force of the physical properties. Substantial band structure calculations were thus carried out with the help of density functional theory using the full-potential local-orbital method (FPLO) in the fully relativistic mode. At the Fermi level, the valence electrons of all the constituents U $5f$ ($6d$), Cr/Ti/V $3d$, Ge $4sp$ participate to the subbands, but the main contribution comes from the U $5f_{5/2}$ states which are slightly delocalized due to hybridization with the T $3d$ states. The results of the band structure calculations nicely reproduced the experimental data on the physical properties outlining the main influence of the T atoms on the magnetic and electronic behaviors of the U_3TGe_5 with $T = Ti, V$ and Cr compounds. Noteworthy, the bandplots of both U_3TiGe_5 and U_3VGe_5 in the magnetically ordered states, reproduced with the help of the orbital polarization correction, exhibit many peculiarities of Dirac-cone-like structures around the Fermi level.

Such assumption of the presence of the Dirac-cones needs further experimental evidence.

Acknowledgments

Francis Gouttefangeas and Loïc Joanny are acknowledged for SEM images and EDS analyses performed on the CMEBA platform belong to the ScanMAT unit (UMS 2001, University of Rennes 1), which received a financial support from the European Union (CPER-FEDER 2007-2014). The Computing Centre at the Institute of Low Temperature and

Structure Research of the Polish Academy of Sciences in Wrocław is acknowledged for use of the supercomputers and technical support. This work is partly supported by a CNRS-PAN PICS project (International Program for Scientific Cooperation) in 2015-2017.

References

- [1] S. S. Saxena, P. Agarwal, K. Ahilan, F. M. Grosche, R. K. W. Hasselwimmer, M. J. Steiner, E. Pugh, I. R. Walker, S. R. Julian, P. Monthoux, G. G. Lonzarich, A. Huxley, I. Sheikin, D. Braithwaite, J. Flouquet, Superconductivity on the border of itinerant-electron ferromagnetism in UGe_2 , *Nature* 406 (2000) 587-592.
- [2] D. Aoki, A. Huxley, E. Ressouche, D. Braithwaite, J. Flouquet, J.-P. Brison, E. Lhotel, C. Paulsen, Coexistence of superconductivity and ferromagnetism in URhGe, *Nature* 413 (2001) 613-616.
- [3] N. T. Huy, A. Gasparini, D. E. De Nijs, Y. Huang, J. C. P. Klaasse, T. Gortenmulder, A. de Visser, A. Hamann, T. Görlach, H. von Löhneysen, Superconductivity on the border of weak itinerant ferromagnetism in UCoGe, *Phys. Rev. Lett.* 99 (2007) 067006.
- [4] D. Aoki, A. Huxley, E. Ressouche, I. Sheikin, J. Flouquet, J.-P. Brison, C. Paulsen, Superconductivity in two itinerant uranium ferromagnets: UGe_2 and URhGe, *J. Phys. Chem. Solid.* 63 (2002) 1179-1182.
- [5] P. Boulet, G.M. Gross, G. André, F. Bourée, H. Noël, Crystal and magnetic structure of new ternary uranium intermetallics: U_3TiX_5 (X= Ge, Sn), *J. Solid State Chem.* 144 (1999) 311-317.
- [6] M. Potzschke, K. Schubert, Zum Aufbau einiger zu T4–B3 homologer und quasihomologer Systeme. I. Die Systeme Titan–Gallium, Zirkonium–Gallium und Hafnium– Gallium, *Z. Metallkd.* 53 (1962) 474-488.
- [7] F. Wastin, J.-C. Spirlet, J. Rebizant, Progress on solid compounds of actinides, *J. Alloys Compd.* 219 (1995) 232-237.
- [8] A. Palenzona, P. Manfrinetti, The phase diagram of the U-Sn system, *J. Alloys Compd.* 221 (1995) 157-160.
- [9] P. Boulet, M. Potel, J.C. Levet, H. Noël, Crystal structure and magnetic properties of the uranium germanide U_5Ge_4 , *J. Alloys Compd.* 262/263 (1997) 229-234.
- [10] P. Villars, K. Cenzual, Pearson's Crystal Data: Crystal Structure Database for Inorganic Compounds (on DVD), Release 2016/17, ASM International, Materials Park, Ohio, USA

- [11] M. Brylak, W. Jeitschko., U_3TiSb_5 , U_3VSb_5 , U_3CrSb_5 , and U_3MnSb_5 with "anti" Hf_5Sn_3Cu type structure, *Z. Naturforsch. B* 49 (1994) 747-752.
- [12] V. Tkachuk, C. P. T. Muirhead, A. Mar, Structure and physical properties of ternary uranium transition-metal antimonides U_3MSb_5 ($M = Zr, Hf, Nb$), *J. Alloys Compd.* 418 (2006) 39-44.
- [13] A. Mar, O. Tougait, M. Potel, H. Noël, E.B. Lopes, Anisotropic transport and magnetic properties of ternary uranium antimonides U_3ScSb_5 and U_3TiSb_5 , *Chem. Mater.* 18 (2006) 4533-4540.
- [14] J. Rodriguez-Carvajal, Recent advances in magnetic-structure determination by neutron powder diffraction, *Physica B* 192 (1993) 55-69.
- [15] SADABS: Area-Detector Absorption Correction; Siemens Industrial Automation, Inc.: Madison, WI, 1996.
- [16] G. M. Sheldrick, Crystal structure refinement with SHELXL, *Acta Crystallogr. C* 71 (2015) 3-8.
- [17] (a) K. Koepnik, H. Eschrig, Full-potential nonorthogonal local-orbital minimum-basis band-structure scheme, *Phys. Rev. B* 59, (1999) 1743-1757; <http://www.FPLO.de>; (b) H. Eschrig, M. Richter, I. Opahle, in *Relativistic Electronic Structure Theory, Part 2. Applications*, ed. P. Schwerdtfeger, *Theoretical and Computational Chemistry, Vol. 14* (Elsevier, Amsterdam, 2004), 723.
- [18] J. P. Perdew, Y. Wang, Pair-distribution function and its coupling-constant average for the spin-polarized electron gas, *Phys. Rev. B* 45 (1992) 13244.
- [19] L. Nordström, M. S. S. Brooks, B. Johansson, Calculation of orbital magnetism and magnetocrystalline anisotropy energy in YCo_5 , *J. Phys.:Cond. Matter* 4 (1992) 3261-3272.
- [20] J. P. Perdew, K. Burke, M. Ernzerhof, Generalized gradient approximation made simple, *Phys. Rev. Lett.* 77 (1996) 3865-3868.
- [21] T. Le Bihan, H. Noël, Characterization of novel ternary uranium silicides and germanides with the $U_2Mo_3Si_4$ structure type in the U-(Mo, W, V)-(Si, Ge) systems, *J. Alloys Compd.* 227 (1995) 44-48.
- [22] P. Boulet, A. Daoudi, M. Potel, H. Noël, Crystal structure and magnetic behavior of the uranium monogermanide UGe , *J. Solid State Chem.* 129 (1997) 113-116.
- [23] P. Boulet, A. Daoudi, H. Noël, G. M. Gross, G. André, F. Bourée, Crystal and magnetic structure of the uranium digermanide UGe_2 , *J. Alloys Compd.* 247 (1997) 104-108.

- [24] T. Le Bihan, H. Noël, P. Rogl, Synthesis and characterization of novel ternary uranium germanides with niobium and tantalum, *J. Alloys Compd.* 213/214 (1994) 540-544.
- [25] G. M. Gross, P. Boulet, H. Noël, Isothermal section of the phase diagram uranium–titanium–germanium at 1000°C, *Mater. Res. Bull.* 34 (1999) 1929–1933.
- [26] R. Marazza, R. Ferro, G. Rambaldi, G. Zanicchi, Some phases in ternary alloys of Th and U with the $Al_4Ba-ThCu_2Si_2$ -type structure, *J. Less-Common Met.* 53 (1977) 193-197.
- [27] T.B. Massalski, H. Okamoto, P.R. Subramanian, L. Kacprzak (Eds.), *Binary Alloy Phase Diagrams*, vols. 1–3, second ed., ASM International, 1990.
- [28] E. S. R. Gopal “Specific heat at low temperatures” Plenum Press, New York, 1966.
- [29] A. Pikul, R. Troć, A. Czopnik, H. Noël, Low-temperature specific heat of uranium germanides, *J. Magn. Magn. Mater.* 360 (2014) 217-221.
- [30] N. F. Berk, J. R. Schrieffer, Effect of ferromagnetic spin correlations on superconductivity, *Phys. Rev. Lett.* 17 (1966) 433-435.
- [31] S. Doniach, S. Engelsberg, Low-temperature properties of nearly ferromagnetic Fermi liquids, *Phys. Rev. Lett.* 17 (1966) 750-753.
- [32] R. J. Trainor, M. B. Brodsky, H. V. Culbert, Specific heat of the spin-fluctuation system UAl_2 , *Phys. Rev. Lett.* 34 (1975) 1019-1022.
- [33] A. J. Arko, M. B. Brodsky, W. J. Nellis, Spin fluctuations in plutonium and other actinide metals and compounds, *Phys. Rev. B* 5 (1972) 4564-4569.
- [34] M. S. Wire, J. D. Thompson, Z. Fisk, Influence of spin fluctuations on the electrical resistance of UAl_2 and UPt_3 at high pressures and low temperatures, *Phys. Rev. B* 30 (1984) 5591-5595.
- [35] C. Geibel, S. Thies, D. Kaczorowski, A. Mehner, A. Grauel, B. Seidel, U. Ahlheim, R. Helfrich, K. Petersen, C. D. Bredl, F. Steglich, A new heavy-fermion superconductor: UNi_2Al_3 , *Z. Phys. B* 83 (1991) 305-306.
- [36] J.-M. Fournier, E. Gratz, in *Handbook on the Physics and Chemistry of Rare Earths*, ed. K. A. Gschneidner, Jr., L. Eyring, G. H. Lander, G. R. Choppin, North-Holland, Amsterdam, (1993) Vol. 17, 409.
- [37] N. H. Andersen, H. Smith, Electron-magnon interaction and the electrical resistivity of Tb, *Phys. Rev. B* 19 (1979) 384-387.
- [38] P. A. Beck, H. Claus, Density of states information from low temperature specific heat measurements, *J. Res. Natl. Stand. Sec. A.* 74 (1970) 449-454.

- [39] O. Merabiha, T. Seddik, R. Khenata, G. Murtaza, A. Bouhemadou, Y. Takagiwa, S. Bin Omran, D. Rached, The effects of 5f localization on the electronic and magnetic properties of the hexagonal U_3ZrSb_5 , *J. Alloys Compd.* 586 (2014) 529-535.
- [40] M. T. Greenaway, E. E. Vdovin, A. Mishchenko, O. Makarovskiy, A. Patané, J. R. Wallbank, Y. Cao, A. V. Kretinin, M. J. Zhu, S. V. Morozov, V. I. Fal'ko, K. S. Novoselov, A. K. Geim, T. M. Fromhold, L. Eaves, *Nature Phys.* 11 (2015) 1057-1062.

TABLES AND TABLE CAPTIONS:

Table 1 Temperature of peritectic transformation of the U_3TGe_5 compounds. The values are given with an absolute error of $\pm 5K$.

U_3TGe_5, T	Ti	V	Cr	Mn	Zr	Nb	Mo	Hf	Ta	W
T (K)	1676	1698	1607	1529	1667	1654	1677	-	-	-

Table 2 Single crystal XRD data and structure refinement parameters for U_3VGe_5 and U_3CrGe_5 compounds.

Chemical formula	U_3VGe_5	U_3CrGe_5
Formula weight (g mol ⁻¹)	1127.98	1129.04
Crystal system. space group	Hexagonal. $P6_3/mcm$	
Cell parameters (Å)	a = 8.466(1) c = 5.655(1)	a = 8.427(1) c=5.664(1)
Z. density (g cm ⁻³)	2. 10.698	2. 10.791
Abs. coef. (cm ⁻¹)	913.81	922.98
θ range (°)	4.82° - 41.94°	4.838°- 41.983°
Limiting indices	-14 ≤ h ≤ 10	-15 ≤ h ≤ 10
	-14 ≤ k ≤ 15	-11 ≤ k ≤ 15
	-10 ≤ l ≤ 10	-10 ≤ l ≤ 10
Collected/unique reflections	4789 / 477	7033 / 470
R(int)	0.0955	0.0943
Abs. correction	Semi-empirical, SADABS	
Data / restraints / parameters	477 / 0 / 14	470 / 0 / 14
Goodness of fit on F ²	0.947	1.115
Residual factors* [$I > 2\sigma(I)$]	$R_1 = 0.028$	$R_1 = 0.0309$
	$wR_2 = 0.0506$	$wR_2 = 0.0596$
Largest difference peak/hole (\bar{e} .Å ⁻³)	3.113; -4.576	3.598; -4.845

$$*R(F) = \sum \frac{|F_0| - |F_c|}{|F_c|} \text{ (for } F^2 > 2\sigma(F^2)) \quad wR_2 = \left[\sum w(F_0^2 - F_c^2)^2 / wF_0^4 \right]^{1/2},$$

$$\text{with } w^{-1} = [\sigma^2(F_0^2) + (Ap)^2 + Bp], \quad p = [\max(F_0^2, 0) + 2F_c^2] / 3$$

Table 3 Atomic positions and equivalent isotropic displacement parameters for U_3VGe_5 and U_3CrGe_5 .

Atom	Wyckoff position	x	y	z	$U_{eq}(\text{\AA}^2)$
U(1)	6g	0.6146(1)	0	1/4	0.007(1)
Ge(1)	6g	0.2587(1)	0	1/4	0.007(1)
Ge(2)	4d	1/3	2/3	0	0.007(1)
V(1)	2b	0	0	0	0.005(1)
U(1)	6g	0.6143(1)	0	1/4	0.007(1)
Ge(1)	6g	0.2566(1)	0	1/4	0.008(1)
Ge(2)	4d	1/3	2/3	0	0.007(1)
Cr(1)	2b	0	0	0	0.005(1)

Table 4 Lattice parameters for the U_3TGe_5 series refined from powder XRD data using the Le Bail method.

U_3TGe_5	Ti	V	Cr	Mn	Zr
a (Å)	8.501(1)	8.460(1)	8.418(1)	8.521(1)	8.586(1)
c (Å)	5.713(1)	5.651(1)	5.659(1)	5.738(1)	5.820(1)
U_3TGe_5	Nb	Mo	Hf	Ta	W
a (Å)	8.523(1)	8.453(1)	8.570(1)	8.514(1)	8.452(1)
c (Å)	5.736(1)	5.695(1)	5.824(1)	5.729(1)	5.682(1)

Table 5 Summary of the main physical parameters of U_3TGe_5 for $T = Ti, V, Cr$ and Mo . The equations (1-4) leading to these values are described in the text.

Compd.		Magnetic data					Specific heat data				LDA
	Order	χ_0 ($10^{-2} \text{ cm}^3 \text{ mol}^{-1}$)	μ_{eff} (μ_B)	θ_p (K)	γ or γ^* ($\text{mJ mol}^{-1} \text{ K}^{-2}$)	β or β^* ($\text{mJ mol}^{-1} \text{ K}^{-4}$)	θ_D (K)	α_{AFM} ($\text{mJ mol}^{-1} \text{ K}^{-4}$)	δ ($\text{mJ mol}^{-1} \text{ K}^{-4}$)	T_{sf} (K)	γ_b ($\text{mJ mol}^{-1} \text{ K}^{-2}$)
U_3TiGe_5	FM	-*	2.24*	74*	105	0.7	292	-	-	-	72.2
U_3VGe_5	AFM	3.08	2.64	23	340	0.7 [§]	292 [§]	0.9	-	-	74.5
U_3CrGe_5	SF	3.54	2.22	-54	510	-6.6	-	-	2.8	14	84.0

FM: ferromagnetic; AFM: antiferromagnetic; SF: spin-fluctuator; * from [5]; [§] fixed to U_3TiGe_5 values

FIGURE CAPTIONS :

Fig. 1 (a) Polyhedral view of the crystal structure of U_3VGe_5 ; (b) U zig-zag chains running along the c -axis; (c) extended U network shown in the (a,b) plane. The solid and dotted lines stand for the U-U distances of $4.554(1) \text{ \AA}$ and $5.6(1) \text{ \AA}$, respectively.

Fig. 2 Evolution of the lattice parameters and unit-cell volume of the U_3TGe_5 series as the function of the atomic radius of the transition metal. The solid lines serve as guideline only.

Fig. 3 (a) Temperature variation of inverse molar magnetic susceptibility χ_{mol}^{-1} of U_3VGe_5 measured in an external magnetic field $\mu_0 H$; solid line is a fit of Eq.1 to the experimental data. Upper inset presents molar magnetization $M_{\text{mol}}(T)$ measured in zero-field-cooling (ZFC) and field-cooling (FC) regimes; solid curves serve as guides for the eye and the arrow marks the ordering temperature T_N . Lower inset: M_{mol} vs. H measured in the ordered region with increasing and decreasing magnetic field (open and closed symbols, respectively); straight lines are added to emphasize the linear character of the magnetization below the transition and arrows indicate the direction of field changes. (b) Low temperature dependence of $M_{\text{mol}}(T)$ of U_3VGe_5 taken in various $\mu_0 H$ (for the sake of clarity the values of M_{mol} measured in 4 T are multiplied by 0.25). Inset displays the temperature dependence of real (χ') and imaginary (χ'') components of the AC magnetic susceptibility measured at temperatures below 40 K using AC magnetic field $\mu_0 H_{\text{AC}}$ of a frequency f_{AC} ; solid lines serve as guides for the eye and arrows mark the ordering temperature T_N .

Fig. 4 Temperature variation of χ_{mol}^{-1} of U_3CrGe_5 ; solid line is a fit of the modified Curie-Weiss law to the experimental data. Upper inset presents the low temperature dependence of

M_{mol} . Lower inset displays M_{mol} measured at 2 K with increasing and decreasing magnetic field (open and closed symbols, respectively); arrows indicate the direction of field changes.

Fig. 5 Temperature dependence of specific heat $C_P(T)$ of U_3TiGe_5 , U_3VGe_5 and U_3CrGe_5 . Arrows mark the ordering temperatures. Insets present C_P/T vs. T^2 . Dashed, dotted and solid lines are fits of Eqs. 2, 3, and 4, respectively, to experimental data.

Fig. 6 (a) Temperature variation of electrical resistivity $\rho(T)$ of U_3TiGe_5 , U_3VGe_5 and U_3CrGe_5 . Inset displays the temperature derivatives of the resistivity $d\rho/dT$ plotted as a function of T . (b) Low-temperature dependence of the resistivity of U_3TiGe_5 together with a fit of Eq. 5 to the experimental data.

Fig. 7 Total and partial DOS's of U_3TGe_5 systems with $T = \text{Ti}$ (a), V (b) and Cr (c) calculated for their non-magnetic states (LDA).

Fig. 8 Total and partial spin-polarized DOS's calculated for U_3TiGe_5 (a) and U_3VGe_5 (b) compounds in their ferromagnetic states (LSDA+OPC) and drawn separately for spin-up (positive) and spin-down (negative values) channels.

Fig. 9 Bandplots calculated for non-magnetic (LDA) U_3CrGe_5 (a) and ferromagnetic (LSDA+OPC) U_3TiGe_5 (b) and U_3VGe_5 (c) systems. Note that the energy scales are expanded in parts (b) and (c) with respect to (a). Some Dirac-cone-like structures are selected in red circles.

Fig. 10 Fermi surface sheets of non-magnetic (LDA) states for U_3TiGe_5 (a), U_3VGe_5 (b) and U_3CrGe_5 (c) originating from Kramers double-degenerate bands as well as of ferromagnetic (LSDA+OPC) states for U_3TiGe_5 (d) and U_3VGe_5 (e) coming from Kramers non-degenerate bands. The FS sheets are drawn separately within the hexagonal BZ boundaries. Green (dark) and yellow (light) sides of the surfaces adjoin electron and hole states, respectively.

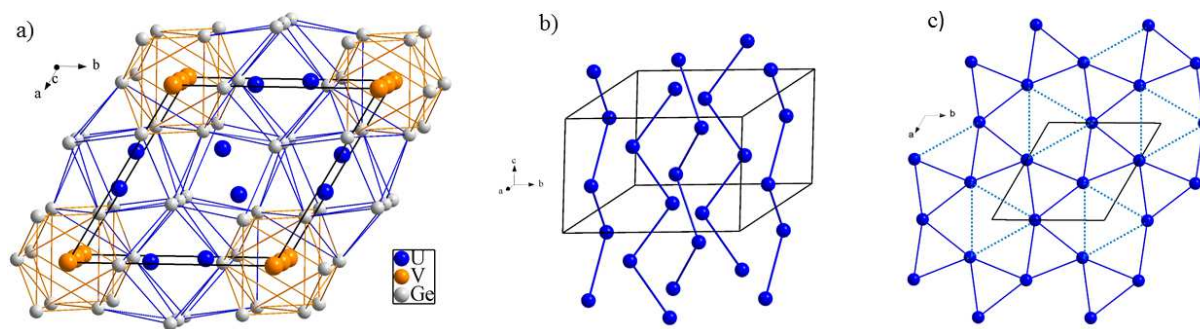


Fig. 1 (a) Polyhedral view of the crystal structure of U_3VGe_5 ; (b) U zig-zag chains running along the c -axis; (c) extended U network shown in the (a,b) plane. The solid and dotted lines stand for the U-U distances of $4.554(1)$ Å and $5.6(1)$ Å, respectively.

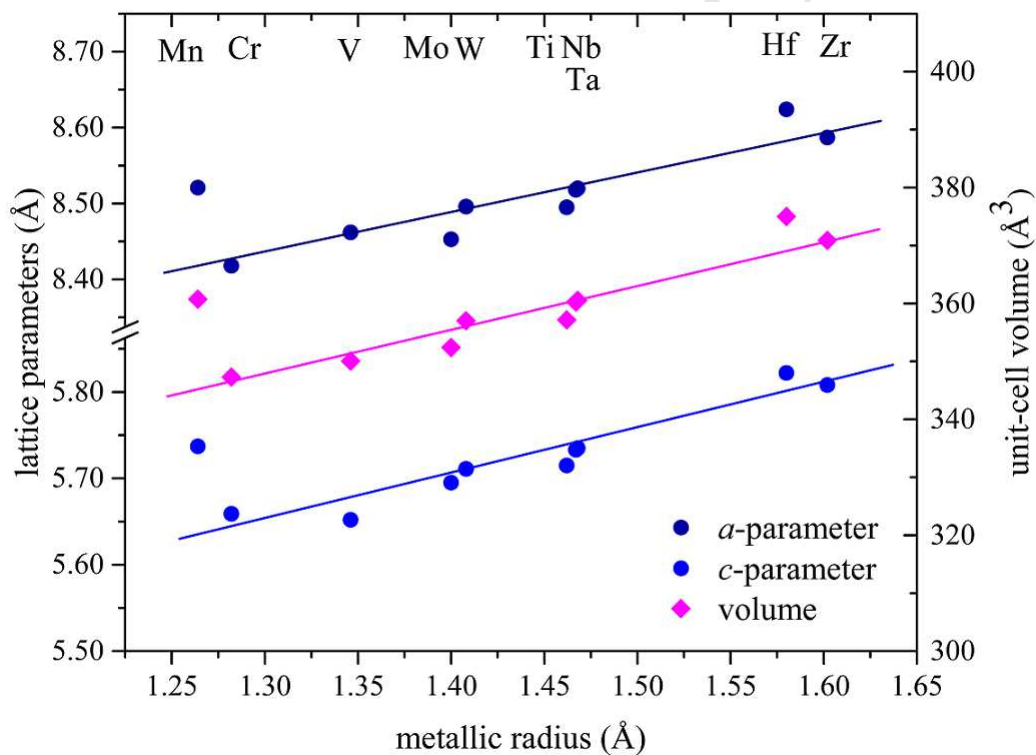


Fig. 2 Evolution of the lattice parameters and unit-cell volume of the U_3TGe_5 series as the function of the atomic radius of the transition metal. The solid lines serve as guideline only.

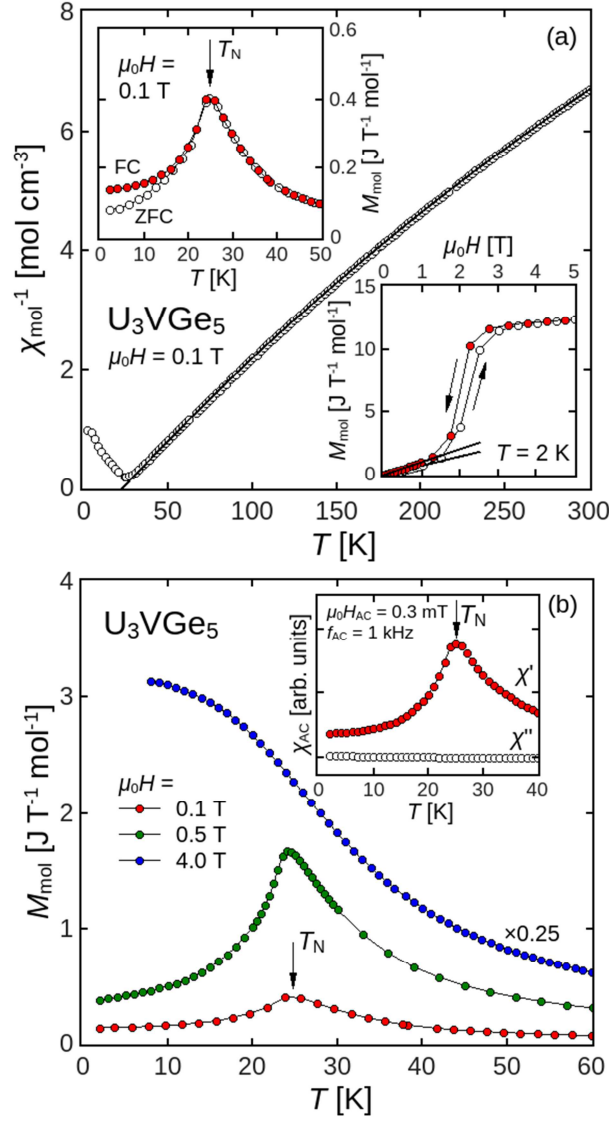


Fig. 3 (a) Temperature variation of inverse molar magnetic susceptibility χ_{mol}^{-1} of U_3VGe_5 measured in an external magnetic field $\mu_0 H$; solid line is a fit of Eq.1 to the experimental data. Upper inset presents molar magnetization $M_{mol}(T)$ measured in zero-field-cooling (ZFC) and field-cooling (FC) regimes; solid curves serve as guides for the eye and the arrow marks the ordering temperature T_N . Lower inset: M_{mol} vs. H measured in the ordered region with increasing and decreasing magnetic field (open and closed symbols, respectively); straight lines are added to emphasize the linear character of the magnetization below the transition and arrows indicate the direction of field changes. (b) Low temperature dependence of $M_{mol}(T)$ of U_3VGe_5 taken in various $\mu_0 H$ (for the sake of clarity the values of M_{mol} measured in 4 T are multiplied by 0.25). Inset displays the temperature dependence of real (χ') and imaginary (χ'') components of the AC magnetic susceptibility measured at temperatures below 40 K using AC magnetic field $\mu_0 H_{AC}$ of a frequency f_{AC} ; solid lines serve as guides for the eye and arrows mark the ordering temperature T_N .

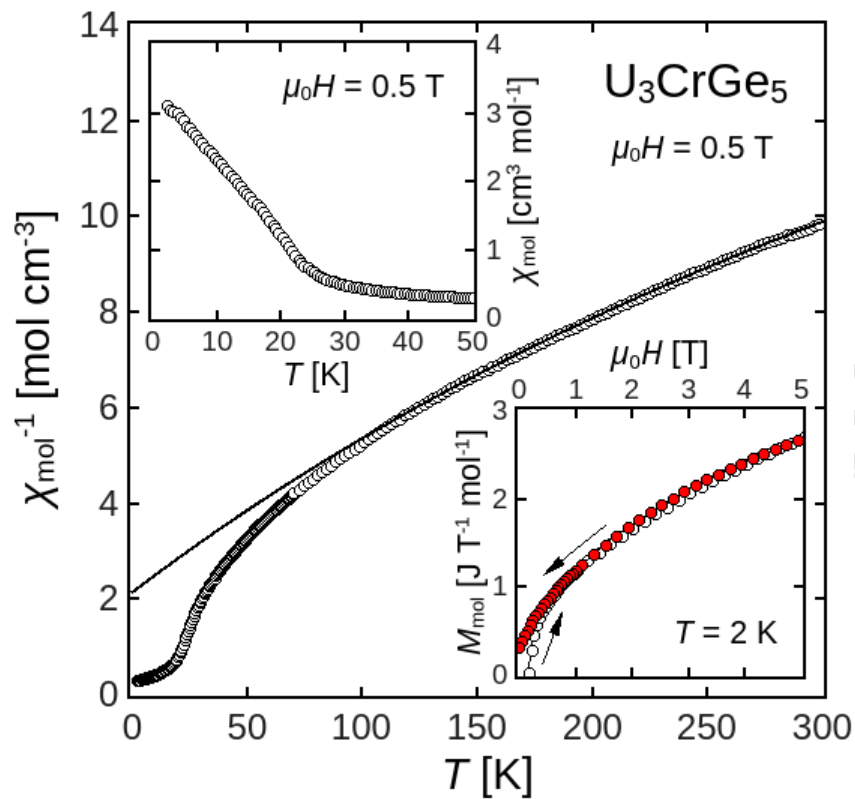


Fig. 4 Temperature variation of χ_{mol}^{-1} of U_3CrGe_5 ; solid line is a fit of the modified Curie-Weiss law to the experimental data. Upper inset presents the low temperature dependence of M_{mol} . Lower inset displays M_{mol} measured at 2 K with increasing and decreasing magnetic field (open and closed symbols, respectively); arrows indicate the direction of field changes.

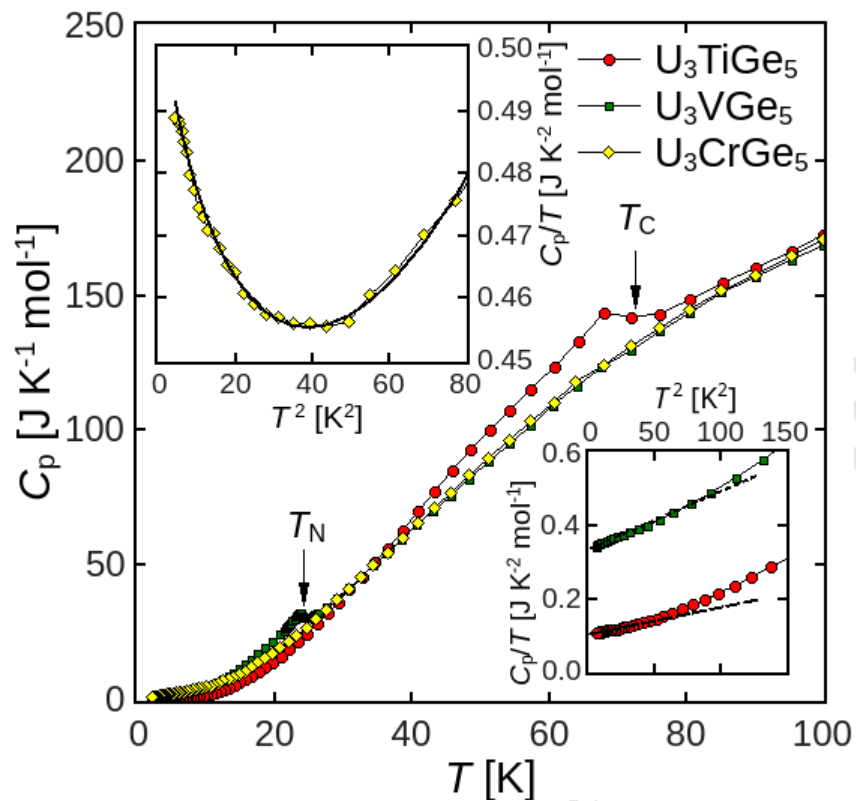


Fig. 5 Temperature dependence of specific heat $C_p(T)$ of U_3TiGe_5 , U_3VGe_5 and U_3CrGe_5 . Arrows mark the ordering temperatures. Insets present C_p/T vs. T^2 . Dashed, dotted and solid lines are fits of Eqs. 2, 3, and 4, respectively, to experimental data.

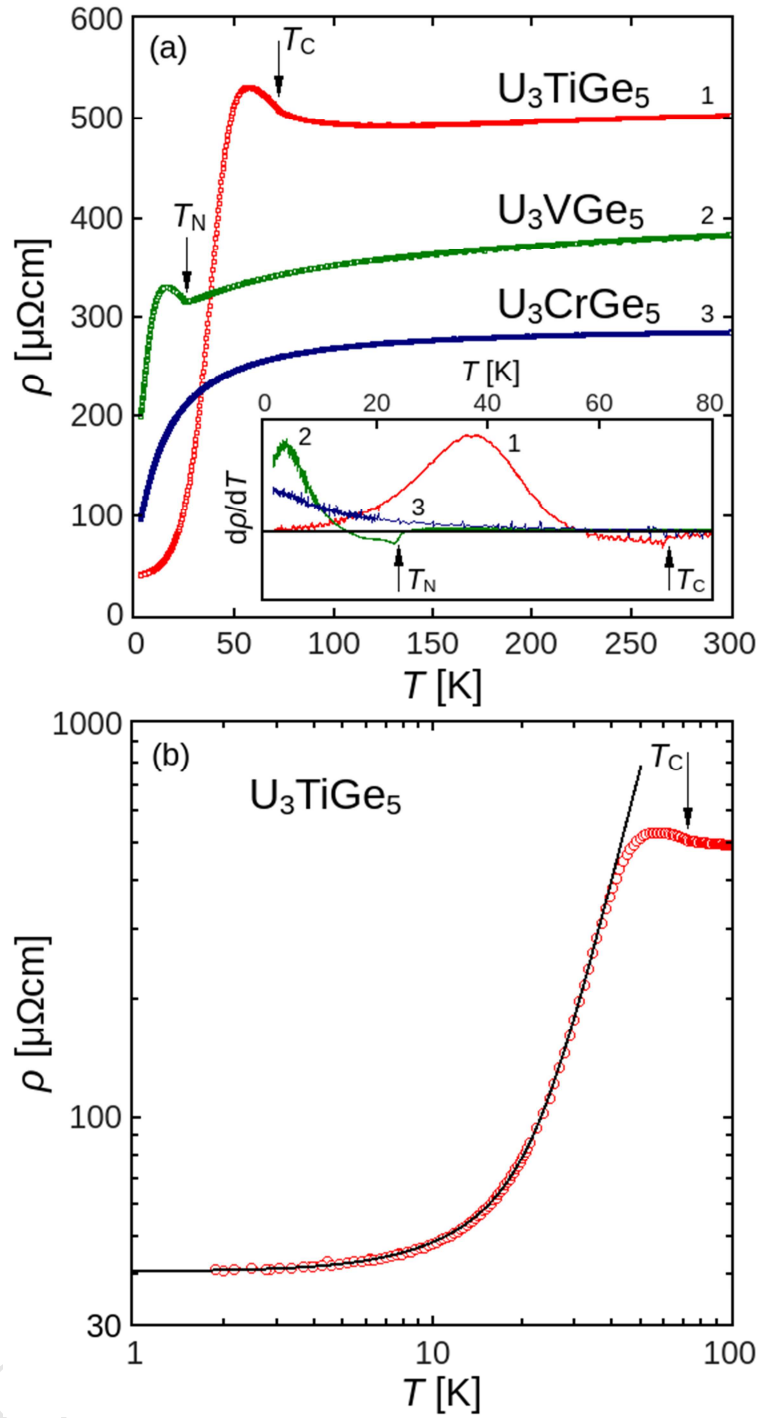


Fig. 6 (a) Temperature variation of electrical resistivity $\rho(T)$ of U_3TiGe_5 , U_3VGe_5 and U_3CrGe_5 . Inset displays the temperature derivatives of the resistivity $d\rho/dT$ plotted as a function of T . (b) Low-temperature dependence of the resistivity of U_3TiGe_5 together with a fit of Eq. 5 to the experimental data.

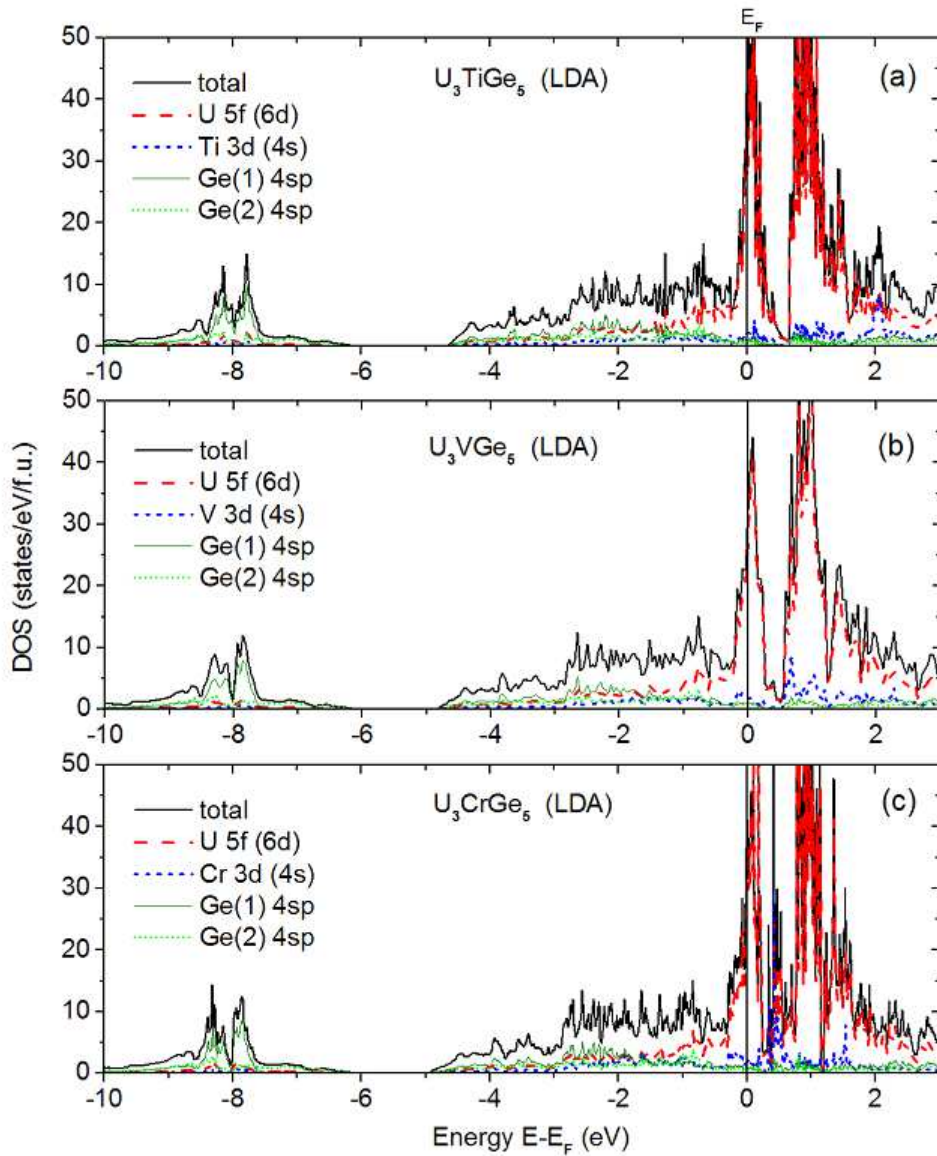


Fig. 7 Total and partial DOS's of U_3TGe_5 systems with $T = Ti$ (a), V (b) and Cr (c) calculated for their non-magnetic states (LDA).

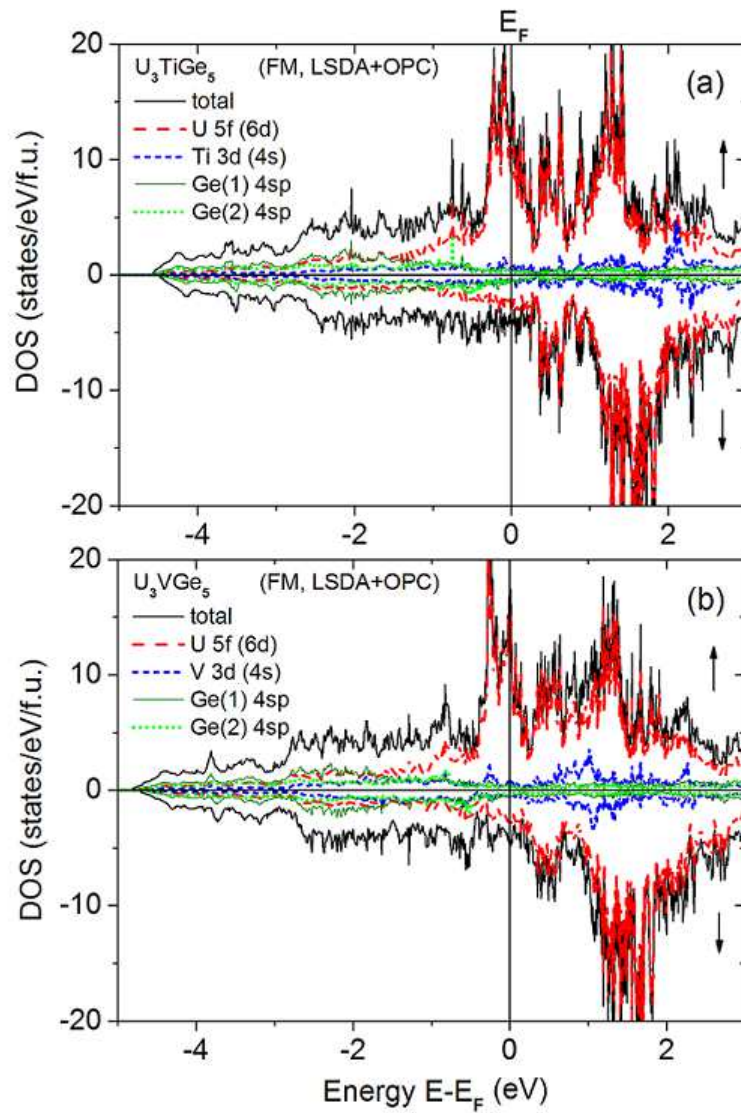


Fig. 8 Total and partial spin-polarized DOS's calculated for U_3TiGe_5 (a) and U_3VGe_5 (b) compounds in their ferromagnetic states (LSDA+OPC) and drawn separately for spin-up (positive) and spin-down (negative values) channels.

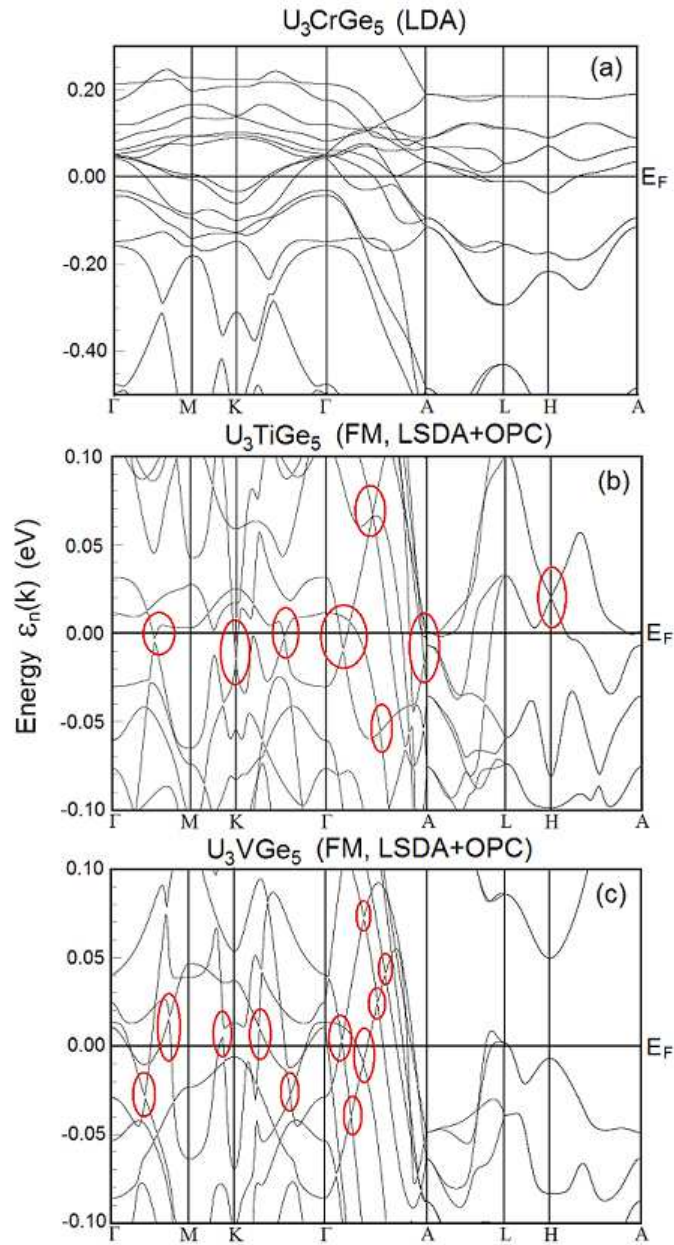


Fig. 9 Bandplots calculated for non-magnetic (LDA) U_3CrGe_5 (a) and ferromagnetic (LSDA+OPC) U_3TiGe_5 (b) and U_3VGe_5 (c) systems. Note that the energy scales are expanded in parts (b) and (c) with respect to (a). Some Dirac-cone-like structures are selected in red circles.

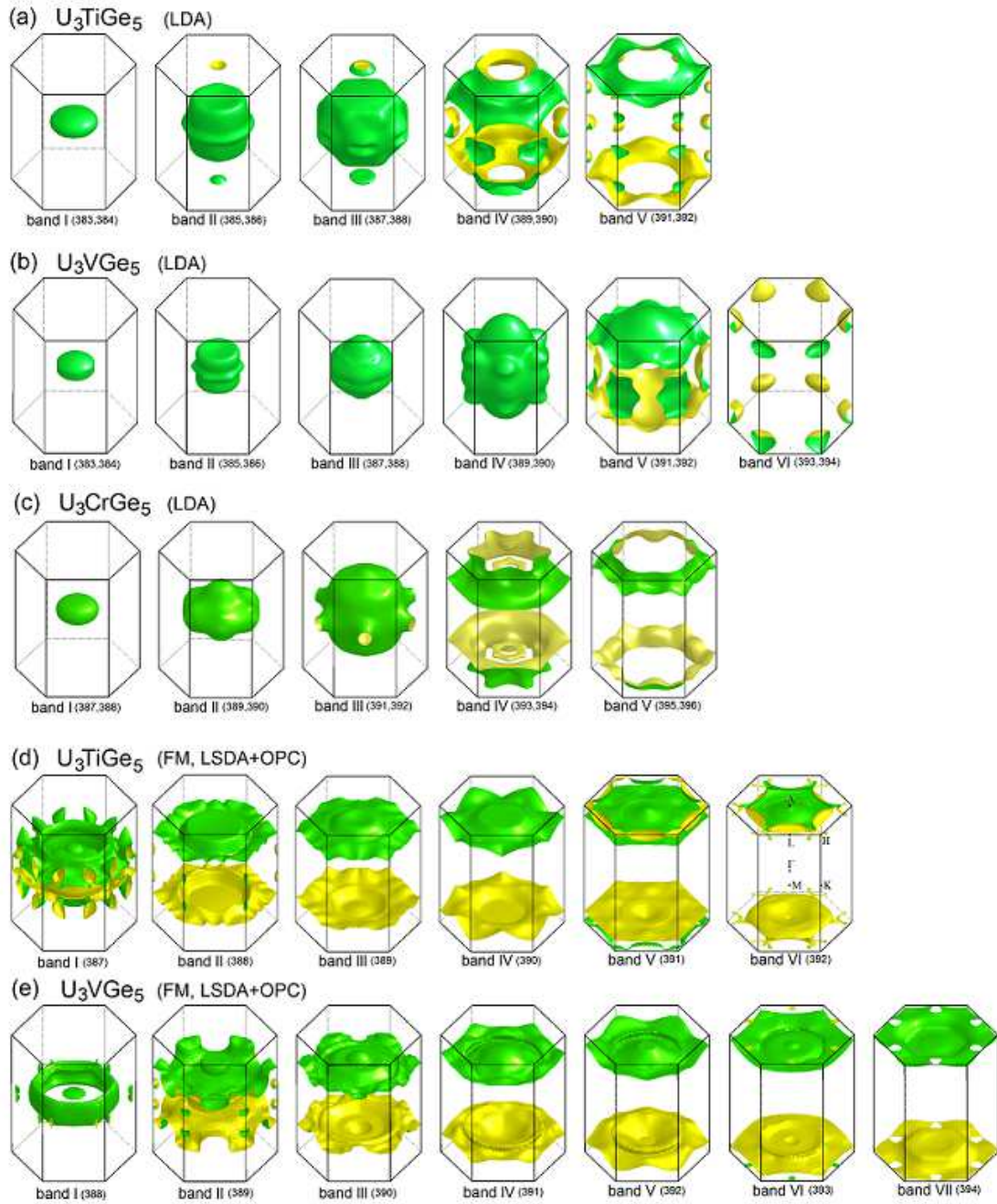


Fig. 10 Fermi surface sheets of non-magnetic (LDA) states for U_3TiGe_5 (a), U_3VGe_5 (b) and U_3CrGe_5 (c) originating from Kramers double-degenerate bands as well as of ferromagnetic (LSDA+OPC) states for U_3TiGe_5 (d) and U_3VGe_5 (e) coming from Kramers non-degenerate bands. The FS sheets are drawn separately within the hexagonal BZ boundaries. Green (dark) and yellow (light) sides of the surfaces adjoin electron and hole states, respectively.